Soft Matter

Accepted Manuscript

ROYAL SOCIETY OF CHEMISTRY

www.rsc.org/softmatter

ARTICLE TYPE www. rsc.org/xxxxxx | XXXXXXXX

Structure of a tractable stochastic mimic of soft particles

Galen T. Craven,[a] Alexander V. Popov,[a] and Rigoberto Hernandez*[a]

Received Xth XXXXXXXXXX 20XX, Accepted Xth XXXXXXXXX 20XX
First published on the web Xth XXXXXXXXXX 200X
DOI: 10.1039/b000000x

The structure and assembly of soft particles is difficult to characterize because their interpenetrability allows them to be packed at ever higher density albeit with an increasing penalty in energy and/or pressure. Alternatively, the use of impenetrable particles (such as hard spheres) as a reference model for soft particles can fail because the packing densities are limited by the impossibility of complete space filling. We recently introduced the stochastic penetration algorithm (SPA) so as to allow for the computationally efficient integration of hard sphere models while including overlaps seen in soft interactions [Craven *et al., J. Chem. Phys.*, 2013, **138**, 244901]. Moving beyond the initial one-dimensional case studied earlier, we now consider the spatial properties of systems of stochastically penetrable spheres in dimensions $d \leq 3$ through the use of molecular dynamics simulations and analytic methods. The stochastic potential allows spheres to either interpenetrate with a probability δ or collide elastically otherwise. For $\delta > 0$ the particles interpenetrate (overlap), reducing the effective volume occupied by the particles in the system. We find that the occupied volume can be accurately predicted using analytic expressions derived from mean field arguments for the particle overlap probabilities with the exception of an observed clustering regime. This anomalous clustering behavior occurs at high densities and small δ. We find that this regime is coincident with that observed in deterministic penetrable models. The behavior of the stochastic penetrable particles also indicates that soft particles would be characterizable through a single reduced parameter that captures their overlap probability.

1 Introduction

The aggregation of small molecular motifs into macromolecular structures gives rise to assemblies and materials with distinct emergent behavior. For processes in which intermolecular forces drive self-assembly, such as polymerization and colloidal flocculation, a theoretical formulation is often intractable from microscopic statistical mechanics due to the complex spatial arrangements of the resulting compositions. The study of such systems is often relegated to purely computational methods, but because of the large number of atoms of which they are composed, macromolecules are difficult to simulate on relevant biological and chemical length scales. The computationally taxing procedure of simulating large systems can be accelerated by reducing the atomic degrees of freedom to a coarse-grained description.[1–3] In the coarse-grained picture, macromolecules can be treated as overlapping particles when soft interaction potentials allow them to interpenetrate relative to their radius of gyration. The complex nature of soft matter interactions is manifested in systems with rheological and structural properties that are absent in simple fluids.[4–6] Previous modeling of soft matter systems using a class of potentials that are finite valued at the origin, bounded potentials, has elucidated the phase behavior and structure of colloid suspensions,[7] polymer-colloid mixtures,[8] star polymers and globular micelles,[9] and dendrimers.[10]

The generalized exponential model of index n (GEM-n),[11,12]

$$V^{\mathrm{GEM}}(r) = \varepsilon \exp\left[-\left(\frac{r}{\sigma}\right)^n\right], \qquad (1)$$

is a prototypical bounded potential. The softness of the potential is specified by the parameter n. For the exponential parameter value $n = 2$, the GEM-2 becomes the Gaussian core (GC) model.[13] The potential (1) is finite valued at $r = 0$ and this gives rise to complex phase and thermodynamic behavior.[14–16] In modeling solutions of micelles, Marquest and Whitten introduced the penetrable sphere (PS) model,[17]

$$V^{\mathrm{PS}}(r) = \begin{cases} 0, & r > \sigma\,, \\ \varepsilon, & r \leq \sigma\,. \end{cases} \qquad (2)$$

The PS model is the limiting form of the GEM as $n \to \infty$, where σ is the diameter of the particle and ε is a finite energy. Only as $\varepsilon \to \infty$ does the PS model take the form of the ubiquitous hard-core (HC) potential,[18–21] otherwise the particles have a non-zero probability to overlap due to the finite nature of the energy barrier. For $\varepsilon = 0$ the PS model represents the ideal gas. The PS model is perhaps the most well-studied bounded potential. Its simplicity allows for the prediction of observables of the system that in most cases are derivable using modified HC arguments.[22–28] As is common with the completely repulsive HC potential, the PS model has been

[a] *Center for Computational Molecular Science and Technology, School of Chemistry and Biochemistry, Georgia Institute of Technology, Atlanta, GA, USA; E-mail: hernandez@chemistry.gatech.edu*

extended to include attractive regions[29–32] for the purpose of modeling complex fluids.

When particles are allowed to interpenetrate due to the bounded nature of the potentials that govern their interactions, the effective volume occupied by the particles in the system is reduced from the non-overlapping value. The spatial properties of such systems are of interest not only in macromolecular assembly, but also in modeling the structure of porous media.[33–36] While the volume occupied by soft-edge potentials, like the GC model, is ill-defined due to the lack of a distinct spatial boundary, the geometric properties of systems with hard-edge boundaries are amenable to both analytic[37–40] and computer studies.[41–44] In order to bridge the dynamics of a system between completely hard and completely ideal behavior, Blum and Stell[45] introduced an abstraction of a bounded potential, called the permeable-sphere model (PSM). Within this model the radial distribution function $g_2(r)$ is constant in the penetrative region (PR) $0 \leq r < \sigma$ and equal to a penetration parameter δ,

$$g_2(r) = \delta. \tag{3}$$

Thus, the PSM uses one parameter to bridge the limiting behaviors.

In this article, a stochastic penetration algorithm (SPA)[46] is used to model penetrative particles. In the SPA, the outcome of collisions between particles are governed by stochastic rules. Through a penetration parameter δ, a mixture of completely hard and completely soft interactions are constructed. The PSM model can be equated to the SPA model only in the limit of infinite dilution. For finite densities, the mixing of stochastic collision events in the SPA generates complex spatial configurations and non-linear behavior for $g_2(r)$ in the PR and thus Eq. (3) does not hold. The dynamics of single-particle trajectories evolved through the SPA are non-Newtonian as particles are allowed to enter classically prohibited regions subject to the outcome of a stochastic variable. However, by combining these hard and soft collision outcomes, the SPA generates ensemble averages that retain the pertinent features of analogous deterministic systems, such as the PS model.

In coarse-grained systems that are governed by imposed Hamiltonian dynamical rules, the probability of entering a repulsive potential region is dependent on the relative velocity of the two colliding particles.[25] If the relative velocity between a colliding pair is below the respective energy threshold for that region, the result is a turning point for soft-edge potentials like the GC model, or an impulsive elastic collision in hard-edge potentials such as the PS model.

In the SPA model, the kinetic energy of a colliding pair plays no role in the penetration process. A set of particles with a relative velocity of small magnitude will sometimes overlap, traversing the now penetrable core. Moreover, a set of particles with large kinetic energy can be repelled by the stochastic collision outcome. The probability of penetration is thus uniformly distributed over the entire energy distribution. The ensemble average of these outcomes generates spatial configurations that are analogous to those found by deterministic bounded potentials such as the PS model. The effective pairwise potential is determined by δ. It replaces the detailed forces in the interaction (or collision) region when moving from the all-atom to CG representations. Thus the SPA is a HC model augmented only by a single pairwise parameter, characteristic of a particles softness, connecting deterministic systems governed by Newtonian mechanics to a stochastic system governed by non-Newtonian mechanics.

When the particles are allowed to overlap, a fundamental observable is the volume fraction ϕ occupied by the particles in the system. We find that ϕ can be predicted using probabilistic arguments and that the system's structural behavior is approximately that of deterministic soft potentials. Thus, when a system's degrees of freedom are coarse-grained, the representative equations of motion can be considered probabilistically as well as deterministically. This result has direct applications in modeling macromolecular assemblies where, previously, deterministic bounded potentials have been utilized to probe the spatial structure at the coarse-grained level.

The paper is outlined as follows: The numerical methods used to simulate and measure the volume occupied by a system of particles governed by a stochastic collision rule are described in Sec. 2. Their structure can be characterized by the radial distribution function $g_2(r)$. A mapping of $g_2(r)$ between the SPA and soft-particle systems is used in Sec. 3 to obtain a correspondence between an SPA model with N-body penetration parameter ζ to a soft-particle system with pairwise softness δ . Analytic theories capable of predicting the occupied volume in dimension $d \leq 3$ for SPA particles are presented in Sec. 4 and tested by comparison between the results measured from molecular dynamics (MD) in Sec. 5. Finally, in Sec. 6, we conclude by summarizing the extent to which the SPA model can be used to obtain structure and dynamics of corresponding soft-particle systems, and the extent to which coarse-grained models can be enhanced through the use of the SPA.

2 Numerical Methods

2.1 Model and Simulation Details

Dynamical simulations have been performed on a system of $N = 1000$ spheres with each sphere having a mass m and diameter σ. These simulations were performed in a d-dimensional periodic hypercube with sides of length L. The volume of a single sphere in dimension d is

$$v^{(d)} = \frac{\pi^{d/2}}{\Gamma(1+d/2)} \left(\frac{\sigma}{2}\right)^d. \tag{4}$$

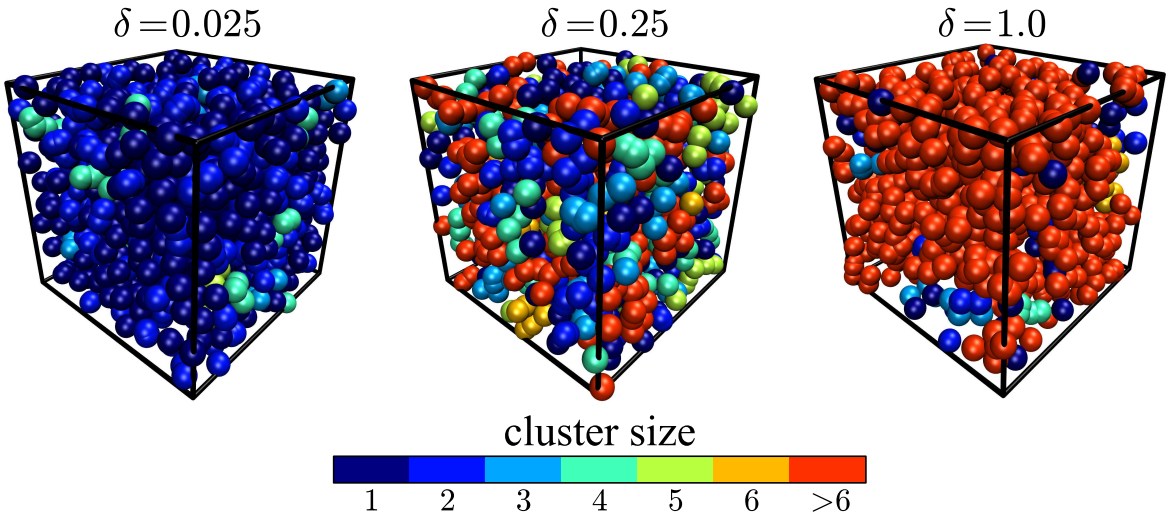

Fig. 1 Selected spatial configurations of $N = 1000$ spheres at $\phi_0 = 0.4$ for $\delta = 0.025$ (left), $\delta = 0.25$ (middle), and $\delta = 1$ (right). The particles are colored according to cluster size N_c.

The HC volume fraction ϕ_0 is the occupied volume fraction of the system when no spheres overlap. In dimension d, the HC volume fraction is

$$\phi_0^{(d)} = \frac{N v^{(d)}}{L^d}. \tag{5}$$

If the spheres are allowed to overlap due to softness in the governing potentials, ϕ_0 is an upper bound to the actual volume fraction ϕ, i.e., $\phi \leq \phi_0$. In simulation, the box volume L^d is changed to reach the target ϕ_0 value while keeping N constant. In the SPA, penetrability is realized by using a single parameter $0 \leq \delta \leq 1$. The limiting values of this parameter, $\delta = 0$ and $\delta = 1$, correspond to the HC and the ideal behavior limits, respectively.

The SPA algorithm is implemented as follows:

1. *For every MD trajectory a value of the penetration probability $\delta \in [0,1]$ is preassigned and maintained throughout the trajectory.*

2. *When a pair of spheres i and j collide at time $t_{\rm col}$, a random number $a_{ij}(t_{\rm col}) \in [0,1]$ is generated from a uniform distribution. This random number determines, upon its comparison to δ, whether or not the pair of particles will interact. If $a_{ij}(t_{\rm col}) > \delta$, they interact via a hard potential; otherwise the particles penetrate each other without interacting.*

3. *For the overlapping particles which do not interact, this relationship between $a_{ij}(t_{\rm col})$ and δ is maintained until $r_{ij} > \sigma$, i.e. the zero interaction potential is kept until the pair breaks apart.*

4. *If the same pair of particles (i, j) undergoes a new collision at time $t_{\rm col} + \tau$, then a new random number $a_{ij}(t_{\rm col} + \tau)$ is generated and the acceptance algorithm is repeated.*

The SPA procedure generates the following stochastic potential between spheres i and j:

$$V_{ij}^{\rm SPA}(r) = \begin{cases} 0, & r > \sigma\,, \\ 0, & r \leq \sigma \text{ and } a_{ij}(t_{\rm col}) < \delta\,, \\ \infty, & r \leq \sigma \text{ and } a_{ij}(t_{\rm col}) > \delta\,, \end{cases} \tag{6}$$

with the random number a_{ij} giving rise to the stochastic nature of the interactions. The potential (6) is used to construct all pairwise interactions in the SPA simulations.

When the stochastic interaction variable $a_{ij}(t_{\rm col}) < \delta$ the particles penetrate each other without interacting leading to pairwise ideal behavior. For trajectories with $\delta = 1$, all pairwise interactions are ideal. In this limit, the structure and dynamics are completely ideal with no spatial correlation between particles.

For trajectories with $\delta = 0$, all pairwise interactions are governed by a HC potential and the dynamics observed are that of a d-dimensional hard sphere system. For $\delta > 0$, the particles can take on overlapping configurations. When the particles overlap, clusters are formed. The size $N_c(i)$ of a cluster is defined by the number of spheres connected by overlaps to i other particles, self-inclusive.[27] As illustrated in Fig. 1, the distribution of cluster sizes is strongly influenced by the value of δ. At small δ the system consists of mostly monomers and dimers. For intermediate δ, higher order oligomers are formed. For $\delta = 1$ the particles have no spatial correlation and are Poisson distributed. In this state, the structure of the system is dominated by transient high order clusters.

In the SPA, the positions and velocities of each particle are updated through a time-driven hard-sphere algorithm.[47] When collisions occur ($a_{ij}(t_{\rm col}) > \delta$), they are elastic and thus the total kinetic energy of the system is conserved. The potential energy of the system V is also constant, $V = 0$, as given by (6). For deterministic dynamical systems governed by soft potentials, such as the GEM, the kinetic energy is not conserved and the total energy of the system is varyingly partitioned into the potential and kinetic terms.

The initial positions of the particles are chosen by placing their centers at distinct points on a uniform lattice. The initial velocities are sampled from a Maxwellian distribution corresponding to $T = 300$ K, although for the athermal potential (6) the choice of temperature is arbitrary.

The simulations are partitioned into two stages: an initial spatial relaxation stage and a second sampling stage. The first stage is implemented to achieve a spatially relaxed state. After the initial velocities are assigned, these velocities are rescaled such that the total energy of the system, for every trajectory becomes $dNk_{\rm B}T/2$. The system is then aged for 5×10^5 collisions to achieve a spatially relaxed state (both hard and soft interactions are counted as collisions in this phase). As observed previously,[46] ϕ relaxes to an equilibrium value quickly during this equilibration phase. During a second sampling stage, all statistical data is generated by sampling the system at constant time intervals. The details for the exact methods used to sample the studied observables are discussed in Sections 2.2 and 3.

The HC volume fractions chosen for the study in one dimension were in the range $\phi_0 \in [0.125, 0.968]$. A one-dimensional gas does not exhibit a phase transition[48] and therefore the system remains in the isotropic phase within this range of volume fractions. An isotropic-solid phase transition occurs for HC systems only in dimensions greater than one.

A system of hard disks in two dimensions undergoes an isotropic-hexatic phase transition at $\phi_0 \approx 0.7$ and a hexatic-solid phase transition at $\phi_0 \approx 0.73$.[49,50] The HC volume fractions chosen for the study in two dimensions are ranged $\phi_0 \in [0.125, 0.75]$. In three dimensions, freezing occurs at $\phi_0 \approx 0.491$ and melting at $\phi_0 \approx 0.543$ with isotropic-solid coexistence occurring between these two volume fractions.[51–53] In three dimensions we have studied volume fractions $\phi_0 \in [0.1, 0.5]$.

In general, when $\delta \neq 0$, the observed volume fraction ϕ is much less than the HC volume fraction ϕ_0. When the particles are allowed to overlap, the phase boundaries present in HC systems cease to exist and complex phase behavior can occur as the particles form clusters.[12,28,54–56]

2.2 Measurement of the Occupied Volume Fraction

For systems consisting of particles with well-defined spatial boundaries, a fundamental observable is the occupied volume fraction. Through the introduction of an indicator function[40]

$$I(\mathbf{r}) = \begin{cases} 1, & \text{if } \mathbf{r} \in \text{particle phase}, \\ 0, & \text{otherwise}, \end{cases} \tag{7}$$

a spatial coordinate $\mathbf{r}$ can be classified as belonging to the particle phase or the void phase. The occupied volume fraction is the expectation value of the indicator function,

$$\phi = \langle I(\mathbf{r}) \rangle, \tag{8}$$

over the domain of all points $\mathbf{r}$ in the simulation subspace $\mathscr{V}$.

Determination of this volume fraction for a system of overlapping particles is non-trivial and often computationally taxing to measure in simulation. Two of the most used methods to measure ϕ are Monte Carlo (MC) integration[42,57] and the GRID method.[25,41,42]

The MC approach involves generating a large number of random coordinates in $\mathscr{V}$, and checking if those coordinates are overlapped by any particle from the system. The ratio of the number of sampling points that are overlapped to the total number of points generated is ϕ, as given by Eq. (8). The GRID method involves discretizing the sampling space $\mathscr{V}$ into uniform bins. These bins are then probed individually to see if any particle overlaps with the chosen bin. The ratio of the number of occupied bins to that of total bins is ϕ.

The accuracy of both the MC and GRID methods increases with an increasing number of sampling points or bins used. However, the trade-off to this increase in accuracy is an increase in computational time. Thus, the number of sampling points or bins is often chosen such that there is an acceptable balance between statistical accuracy and computational efficiency.

Although algorithms that give an exact measure of the occupied volume are known in one and two dimensions,[46,58] we have used the MC sampling method to maintain a uniform methodology for all dimensions studied. We have found that MC gives an acceptable mix between ease of implementation, computational efficiency, and statistical accuracy. To measure ϕ, for each parameter set $\{\delta, \phi_0\}$, 10^4 frames were integrated using 10^6 sampling points per frame. A single trajectory was evolved to generate the configurations used for integration. Previous studies using 8000 trajectories yielded the same results, up to finite size effects,[46] thus confirming the ergodicity of systems evolving through Eq. (6).

3 Radial Distribution Function and ζ-Mapping

When a macromolecule's atomistic degrees of freedom are reduced to a coarse grained description, the effective potential between the coarse-grained structures can be modeled using bounded potentials. The bounded, i.e., finite, nature of these potentials allows for the centers of mass of the coarse-grained macromolecules to overlap relative to their radius of gyration σ. This leads a characteristic feature in $g_2(r)$ where there is a non-zero probability to find the interacting macromolecules directly on top of each other, i.e., $g_2(0) \neq 0$. This is in contrast with simple fluid interactions in which the excluded volume of the nuclei give zero probability to find the interacting molecules in a completely overlapped state. The softness of the governing coarse-grained potentials leads to cluster formation [12,28,54–56] and complex functional forms for $g_2(r)$ in the penetrative region (PR) defined by r such that $0 \leq r < \sigma$. For systems that evolve through the potential (6), the functional form of $g_2(r)$ depends on the pairwise penetration probability δ and therefore it must be included as a parameter, $g_2 = g_2(r;\delta)$.

In the dilute limit, when three and higher order interactions can be neglected, $g_2(r;\delta)$ is constant in the PR and equal to δ. As the density of the gas is increased multi-body effects dominate the potential of mean force. In the language of the Ornstein-Zernike formalism, indirect contributions dominate the structural assembly whereas the direct contributions leading to $g_2(r) = \delta$ are small. When these indirect contributions are strong, as is the case in dense N-body systems, $g_2(r;\delta) \neq \delta$ due the multi-body effects. The potential of mean force (PMF) $w_2(r;\delta)$ between a pair of particles can be extracted from $g_2(r;\delta)$ through the relationship

$$g_2(r;\delta) = e^{-\beta w_2(r;\delta)}, \tag{9}$$

where $\beta = 1/k_B T$.

Figure 2 shows $g_2(r;\delta)$ for a one-dimensional system at $\phi_0 \in \{0.25, 0.5, 0.75\}$ over various values of δ. For $\phi_0 = 0.25$, the radial distribution function approaches constant behavior for $r < \sigma$. At higher ϕ_0 values, in the PR, $g_2(r;\delta) \neq \delta$ and particles have a propensity to be in overlapped states which is evident by observing that $g_2(0;\delta) \geq g_2(\sigma^-;\delta)$, with the equality holding as $\phi_0 \to 0$. (Note that σ^- and σ^+ correspond to the approach of r to σ from the left or the right, respectively.) The reduced volume state arises from the overlap of effectively-ideal particles into clusters ($N_c \geq 2$). The particles in the cluster are free to overlap at no energy cost as the interaction between them is ideal. If the cluster has HC interactions with a shell of particles surrounding them, the HC interactions push the clustering particles into a completely overlapped state forcing the cluster to minimize the occupied volume. This confinement effect gives rise to the $g_2(0;\delta) \geq g_2(\sigma^-;\delta)$ behavior. It is interesting to note that while particles belonging to the cluster have no intracluster interactions, the characteristic concavity in $g_2(r)$ is also observed in deterministic models in which clustering is brought on by intermolecular and intramolecular interactions. [22–24,56]

The pairwise softness δ can be be mapped to a heuristic N-body softness parameter ζ. to account for multi-body induced effects in the pairwise potential through the weighted distribution of energy states in the PR. In dimension d, we define this parameter as the probability to find a particle in the PR, with respect to a test particle, for a specific value of δ, normalized by the ideal ($\delta = 1$) probability,

$$\zeta_{\rm V}^{(d)}(\delta) = \frac{\int_0^\sigma r^{d-1} e^{-\beta w_2(r;\delta)}\, dr}{\int_0^\sigma r^{d-1} e^{-\beta w_2(r;1)}\, dr}. \tag{10}$$

For $\delta = 0$, $\zeta_{\rm V} = 0$ because particles are not allowed in the PR and for $\delta = 1$, $\zeta_{\rm V} = 1$. Thus, the limiting values of $\zeta_{\rm V}$ are in agreement with the limiting values of δ.

The results given by Eq. (10) in one, two, and three dimensions are shown in Fig. 3(a), (b), and (c), respectively. The trend in $\zeta_{\rm V}^{(d)}$ is the same across all dimensions d. As we will show, ϕ has distinct trends that depend highly on the dimensionality of the system. We conjecture, and illustrate in Sec. 5, that these dimensionally-variant spatial effects can be captured by a different softness parameter,

$$\zeta_{\rm L}(\delta) = \frac{\int_0^\sigma e^{-\beta w_2(r;\delta)}\, dr}{\int_0^\sigma e^{-\beta w_2(r;1)}\, dr}, \tag{11}$$

using line (contour) integrals of the Boltzmann-weighted states over the PR along the one-dimensional line connecting the centers of a given pair of particles. The ζ's defined by Eqs. (10) and (11) are equivalent in one dimension ($d = 1$) but differ dramatically at higher d. As will be seen below, the parameter $\zeta_{\rm L}$ is more effective in following the trends observed for spatial properties, and specifically ϕ, as the system dimensionality is increased.

Figure 4(a) shows $\zeta_{\rm L}$ as a function of δ for a one-dimensional system. The $\zeta_{\rm L}$ values are calculated by numerical integration of Eq. (11) for $g_2(r;\delta)$ values obtained from MD simulations. At the dilute density $\phi_0 = 0.125$, $\zeta_{\rm L}$ weakly deviates from the ideal δ value. As ϕ_0 is increased toward the maximum HC packing fraction, $\phi_0 = 1$, a characteristic shape occurs. For small δ, the $\zeta_{\rm L}$ values deviate strongly from ideal behavior. As δ is increased toward the ideal limit, $\delta = 1$, $\zeta_{\rm L}$ deviates less strongly. This effect is induced by the SPA, as the particles in the system are not strongly correlated when the probability of collision is small.

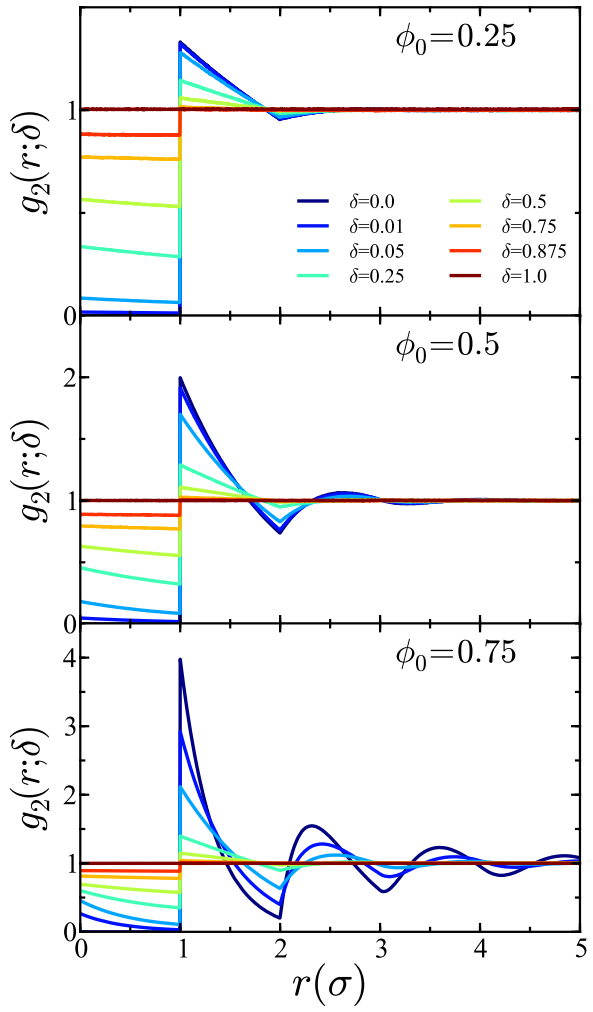

Fig. 2 The radial distribution function $g_2(r;\delta)$ for one-dimensional rods ($d=1$) measured from simulations at various ϕ_0 and δ values using a histogram bin width of $\sigma/300$. The integration was performed for each set of parameters $\{\phi_0,\delta\}$ over a varying number $(5\times10^5-2\times10^6)$ of configurations.

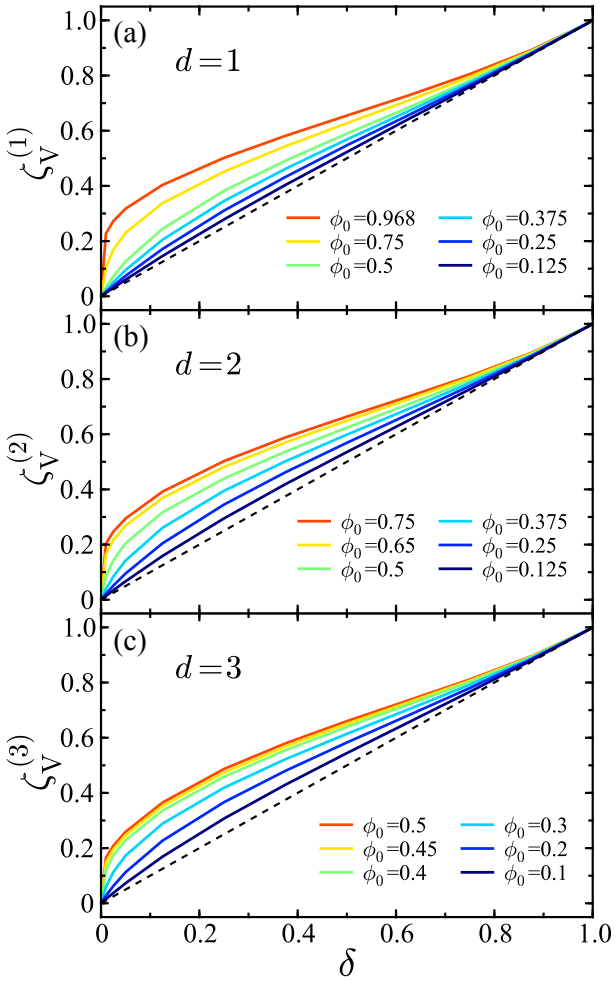

Fig. 3 $\zeta_V^{(d)}$ as a function of δ, at various ϕ_0 values, for systems in (a) $d=1$, (b) $d=2$, and (c) $d=3$ dimensions. The black dashed line corresponds to the infinite dilution limit.

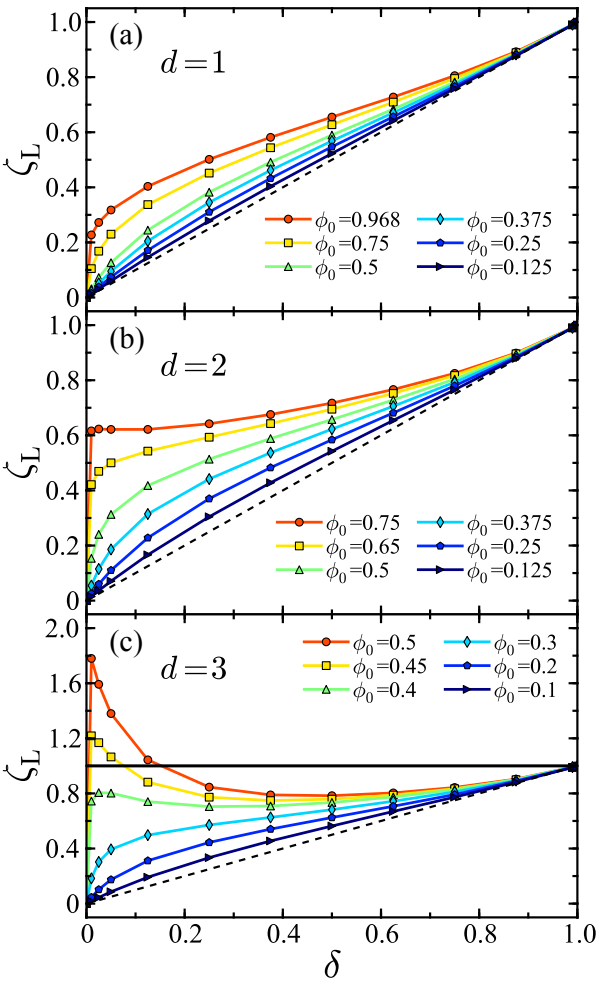

Fig. 4 ζ_L as a function of δ, at various ϕ_0 values, for systems in (a) $d=1$, (b) $d=2$, and (c) $d=3$ dimensions. The black dashed line corresponds to the infinite dilution limit. The black solid line in (c) is the $\zeta_L=1$ upper bound.

In two dimensions, as shown in Fig. 5, the trends of $g_2(r;\delta)$ are generally the same as those seen in one dimension. The HC volume fraction $\phi_0=0.75$ is above the solid phase transition and $g_2(r;0)$ begins to take on the characteristic shape of a solid. For $\phi_0=0.75$ and $\delta=0.01$, $g_2(0;\delta)>g_2(\sigma^+;\delta)$ showing that the density of the system is greatest inside the the PR. This affects ζ_L strongly, as shown in Fig. 4(b) where the ζ_L/δ ratios are larger than those in one dimension for small δ.

In Fig. 6, the measured $g_2(r;\delta)$ functions are shown for a system of three-dimensional spheres at various ϕ_0 and δ values. For small δ and large ϕ_0, highly overlapped states are heavily favored and $g_2(0;\delta)\gg g_2(\sigma^+;\delta)$ with respect to one and two dimensional systems. In this large-ϕ_0, small-δ regime, overlapping configurations dominate in the distribution of particles. This clustering state is analogous to the so-called *"cluster anomaly"* found in the deterministic (GEM-*n*) model.[56] In the SPA it leads to a turnover in the ζ_L function for larger packing fractions ϕ_0 as shown in Fig. 4(c), whereas in one and two dimensional systems ζ_L is a monotonically increasing function of δ at ϕ_0.

The trends observed in $g_2(r;\delta)$ suggest that as the dimensionality is increased, pairs of overlapping particles become more confined by the first solvation shell. For $d=1$, the number of neighboring sites is 2. For a particle to be allowed to leave a cluster, there must either be a cavity available to accommodate the particle, or a neighboring site must switch interaction from HC to ideal, i.e., a random number $a(t_{\rm col})$ generated at the time of collision must be less than δ. With increasing ϕ_0, the probability to find a cavity with enough free volume decreases. Thus, for a particle to leave a cluster it must do so through a stochastic switching of interactions. As the dimensionality is increased, the number of neighboring sites also increases due to the respective packing geometries. With increasing d, the particles in a cluster interact repulsively with more neighbors. This increase in the number of neighbors forces the cluster into a heavily overlapped state. This phenomenon is manifested in the trends of $g_2(r;\delta)$ discussed above.

4 Theory

In this section, we derive two expressions for predicting the occupied volume fraction ϕ of a system of SPA particle with hard core volume fraction ϕ_0. The first one is an analog of an expression derived by Rikvold and Stell (RS)[59,60] for the PSM using the Kirkwood superposition approximation,[61] but now obtained for a system of particles evolving through the SPA. The second expression relies on mean field arguments for the conditional probabilities of finding a pair of particles in an overlapped state as particles are sequentially added to the system.

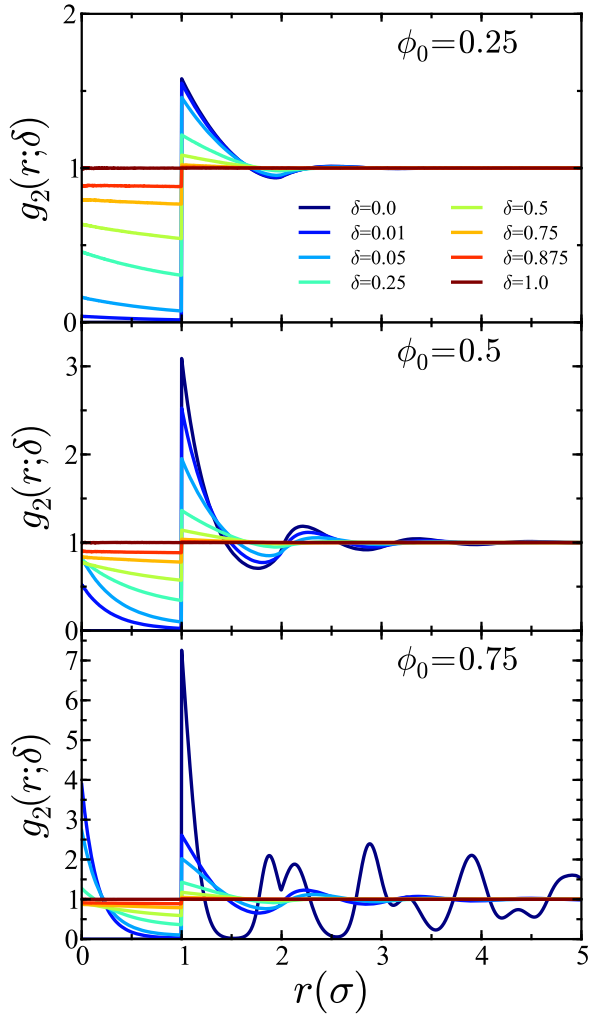

Fig. 5 The radial distribution function $g_2(r;\delta)$ for two-dimensional disks $(d=2)$ measured from simulations at various ϕ_0 and δ values using a histogram bin width of $\sigma/300$. The integration was performed for each set of parameters $\{\phi_0,\delta\}$ over a varying number $(5\times10^5-3\times10^6)$ of configurations.

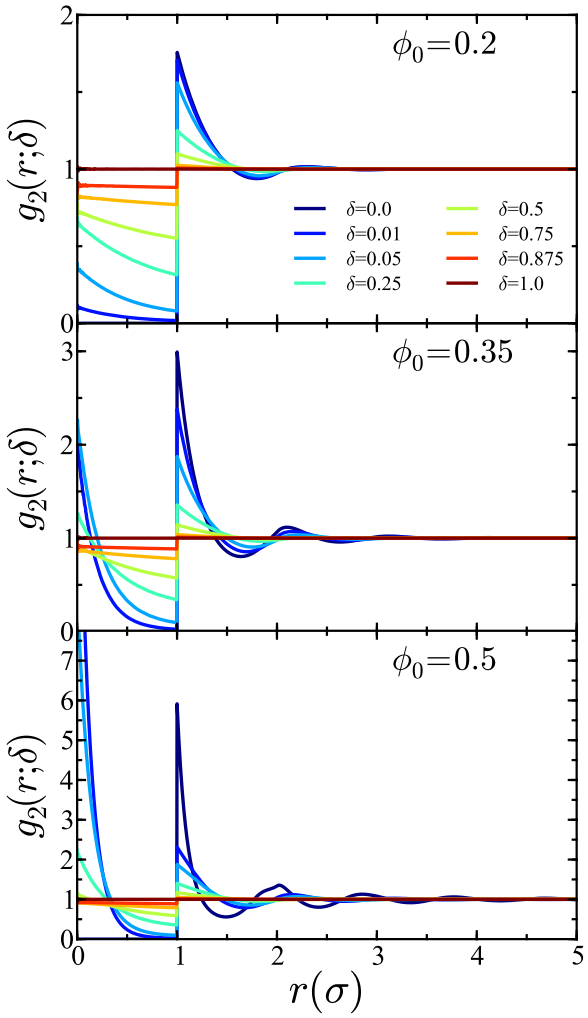

Fig. 6 The radial distribution function $g_2(r;\delta)$ for three-dimensional spheres $(d=3)$ measured from simulations at various ϕ_0 and δ values using a histogram bin width of $\sigma/300$. The integration was performed for each set of parameters $\{\phi_0,\delta\}$ over a varying number $(5\times10^5-3\times10^6)$ of configurations.

4.1 Kirkwood Superposition Approximation for SPA particles

In the PSM,[45] the pair correlation function $g_2(r)$ is taken to be a constant in the PR. In this limit, we can define δ, as used in the SPA model, as that constant, i.e., $g_2(r;\delta)=\delta$. Thus, in analogy with Eqs. (10) and 11, both $\zeta_{\rm V}^{(d)}$ and $\zeta_{\rm L}$, for any dimension, are equal to δ, i.e.,

$$\zeta_{\rm L,V}(\delta)=\delta. \tag{12}$$

This is the limiting case of the SPA model at infinite dilution. To predict ϕ in the PSM, RS also used the Kirkwood superposition approximation[61] for higher-order correlation functions,

$$g_n(\mathbf{r}_1,\ldots,\mathbf{r}_n)=\prod_{1\le i<j\le n} g_2(r_{ij}), \tag{13}$$

e.g.,

$$g_3(\mathbf{r}_1,\ldots,\mathbf{r}_3)=\delta^3, \tag{14}$$

$$g_4(\mathbf{r}_1,\ldots,\mathbf{r}_4)=\delta^6, \tag{15}$$

and in the thermodynamic limit $(N\to\infty, L^d\to\infty, N/L^d = const)$ derived a dimensionally invariant expression for the occupied volume fraction through a power series in ϕ_0,[33,35,59,60]

$$\phi^{\text{RS-SPA}}(\phi_0,\delta)=-\sum_{k=1}^{\infty}\frac{(-\phi_0)^k}{k!}\delta^{\frac{k(k-1)}{2}}, \tag{16}$$

where ϕ_0 is the volume fraction for a HC system. From Eq. (16), the limiting values of δ give,

$$\phi^{\text{RS-SPA}}(\phi_0,0)=\phi_0, \tag{17}$$

$$\phi^{\text{RS-SPA}}(\phi_0,1)=1-e^{-\phi_0}. \tag{18}$$

Equation (17) is the HC volume fraction, given by Eq. (5). Equation (18) is the Poisson distributed result[36,62] for the volume fraction of particles with no spatial correlation at the thermodynamic limit.

Far from the thermodynamic limit (small N), Eq. (16) must be replaced by its finite variant,[46]

$$\phi^{N\text{-SPA}}(N,\phi_0,\delta)=-\sum_{k=1}^{N}\binom{N}{k}\frac{(-\phi_0)^k}{N^k}\delta^{\frac{k(k-1)}{2}}. \tag{19}$$

where $\binom{N}{k}$ is the binomial coefficient, and the last term in the summand is the k-th order correlation function g_k. The difference in Eq. (16) and Eq. (19) lies in coefficients of the ϕ_0 power series. The limiting values of δ in Eq. (19) give

$$\phi^{N\text{-SPA}}(N,\phi_0,0)=\phi_0, \tag{20}$$

$$\phi^{N\text{-SPA}}(N,\phi_0,1)=1-\left(1-\frac{\phi_0}{N}\right)^N. \tag{21}$$

As the thermodynamic limit is approached, $\phi^{N\text{-SPA}}\xrightarrow{N\to\infty}\phi^{\text{RS-SPA}}$.

Multi-body interactions leading to clustered states, can drastically affect ϕ in the SPA model. To account for the indirect, multi-body induced effects, ζ must be used in place of δ. The general Kirkwood approximation for the k-th order correlation function in ζ-space is

$$g_k^{(\zeta)}=(\zeta(\delta))^{\frac{k(k-1)}{2}}. \tag{22}$$

The analog to the finite N-SPA expression, Eq. (19), for ϕ in ζ-space can thus be written as

$$\phi^{\zeta\text{-SPA}}(N,\phi_0,\zeta(\delta))=-\sum_{k=1}^{N}\binom{N}{k}\frac{(-\phi_0)^k}{N^k}g_k^{(\zeta)}. \tag{23}$$

with the replacement from Eq. (22) serving to account for the overlaps between the particles. In practice, the values of ζ can be estimated using either Eq. (10) or Eq. (11). We will refer to these as the $\zeta_{\rm V}$-SPA and the $\zeta_{\rm L}$-SPA, respectively.

4.2 Sequential Iteration Method

A more accurate expression for estimating ϕ was constructed in Ref. 46 through the sequential addition of particles to a hypercube with volume L^d. Although it was derived for the one-dimensional case, all the arguments of this sequential iteration method (SIM) remain valid for systems of d-dimensional penetrable spheres with arbitrary dimension d. Within the SIM approximation, the occupied volume fraction

$$\phi^{\text{SIM}}(N,\phi_0,\zeta(\delta))=\phi^{(N)}, \tag{24}$$

remains a function of N, ϕ_0 and the penetration parameter δ (see Eq. (11) above). The RHS of Eq. (24) is the N-particle limit of the series of occupied volume fractions $\phi^{(n)}$ for n particles. Each such fraction can be written as

$$\phi^{(n)}=1-\prod_{i=1}^{n}Q^{(i)}, \tag{25}$$

where $Q^{(i)}$ is the conditional probability that a random point $x_{\rm R}$ not in the covering of the first $i-1$ particles is also not covered by the i-th particle. These probabilities are found as

$$Q^{(i)}=\sum_{k=0}^{i-1}\binom{i-1}{k}\zeta^{i-k-1}(1-\zeta)^k q_k, \tag{26}$$

where q_k is the probability that $x_{\rm R}$ remains a point in the void phase of an $i-1$ particle system after the i-th particle is added under the condition that the i-th particle has no overlap with at least k other particles.

The probabilities q_k, obtained from a recurrence relation by use of mean field arguments,[46] read

$$q_k = \frac{q_0 - \phi^{(k)}}{1 - \phi^{(k)}}, \tag{27}$$

where q_0 is the probability that the first particle added to the system does not cover the random point x_R:

$$q_0 = \frac{L^d - v^{(d)}}{L^d} = 1 - \frac{\phi_0}{N}, \tag{28}$$

and $v^{(d)}$ is the volume of a single sphere in dimension d, given by Eq. (4).

Through Eqs. (12), (24), (25), (26), and (27) the expression for $\phi^{\rm SIM}(N, \phi_0, \zeta(\delta))$ can be evaluated giving

$$\phi^{\rm SIM}(N, \phi_0, \zeta(\delta)) = 1 - \prod_{i=1}^{N} \left(\sum_{k=0}^{i-1} \binom{i-1}{k} \zeta^{i-k-1} (1-\zeta)^k q_k \right). \tag{29}$$

It gives the correct result in several limiting cases. For example, in the case of hard spheres, where $\delta = 0$, one obtains

$$\phi^{\rm SIM}(N, \phi_0, \zeta(0)) = 1 - q_0 q_1 \cdots q_{N-1} = \phi_0, \tag{30}$$

as one expects for the HC limit from Eq. (20). For fully transparent particles in the $\delta = 1$ limit, the occupied volume fraction is

$$\phi^{\rm SIM}(N, \phi_0, \zeta(1)) = 1 - q_0^N, \tag{31}$$

which is equal to the exact result given by Eq. (21). Thus, at limiting values of δ, the SIM expression is exact. We will refer Eq. (29) as both the ζ_V-SIM and the ζ_L-SIM expression, depending on which ζ parameter is used in calculation.

5 Discussion

5.1 One Dimension

In one dimension, the dynamics are those of a system of rods moving on a line. Shown in Fig. 7 are the results for ϕ given by the N-SPA (19), ζ_L-SPA (23) and ζ_L-SIM (29) expressions. Note that for $d = 1$, $\zeta_L = \zeta_V$.

For dilute systems, ϕ is an approximately linear function of δ and all three analytic predictors give satisfactory results, interpolating approximately linearly between the completely hard ($\delta = 0$) limit and the completely soft Poisson distributed ($\delta = 1$) limit. As ϕ_0 is increased and the system becomes denser, a characteristic feature of ϕ in systems governed by bounded potentials can be seen. As δ is moved slightly from the $\delta = 0$ limit, ϕ decreases drastically due to pressure pushing the particles into overlapped states. In this regime, both the N-SPA and ζ_L-SPA expressions fail to agree with simulation

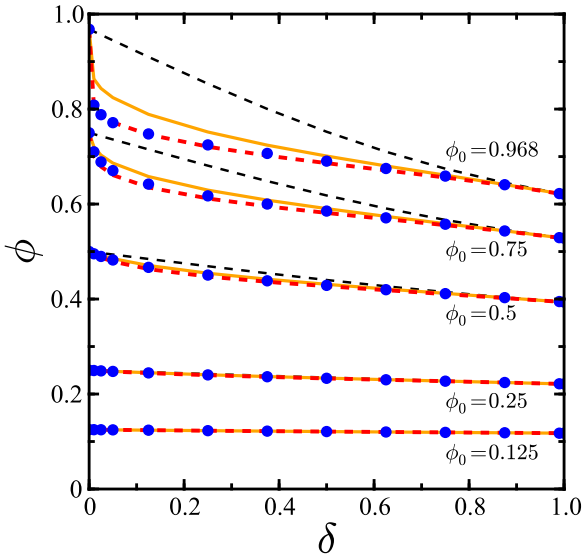

Fig. 7 The occupied volume fraction ϕ as a function of the penetration probability parameter δ in one dimension ($d = 1$). The blue filled circles are the results of MD simulations. The result of the N-SPA expression, given by Eq. (19), is shown as a dashed black curve. The ζ_L-SPA expression, given by Eq. (23), is shown as a solid orange curve. The ζ_L-SIM result, given by Eq. (29), is shown as a dashed red curve.

results while the ζ_L-SIM expression shows excellent agreement. The error between the results measured from MD and ζ_L-SIM expression is $< 1.5\%$ over all values of ϕ_0 and δ. In comparison, the N-SPA expression gives error $> 20\%$ at large ϕ_0 and small δ.

5.2 Two Dimensions

The results for ϕ generated from simulation and analytic theory for a two-dimensional system of disks are shown in Fig. 8. The general trends are the same as in one dimension. When $\delta \neq 0$ the observed volume fraction is decreased from ϕ_0. This decrease is pronounced at high densities and small δ where overlapped states are favored as observed in the PR of $g_2(r; \delta)$ in Fig. 5. The N-SPA expression, which is shown only for $\phi_0 = 0.75$, fails in the large-ϕ_0, small-δ regime while both the ζ_L-SIM and the ζ_L-SPA expressions show agreement with the results measured from MD simulations across all ranges of ϕ_0 and δ studied. The ζ_L-SIM expression gives error in ϕ, with respect to values obtained from MD simulation, of $\approx 5\%$ at large ϕ_0 and small δ, with typical error $< 1\%$ outside of this regime. Interestingly, the dimensionally-scaled ζ_V-SIM expression gives error $\approx 10\%$ at large ϕ_0 and small δ values. This error decreases significantly as δ is increased, but it is always greater than that given by the ζ_L-SIM expression, up to large δ values where the error in both expressions becomes

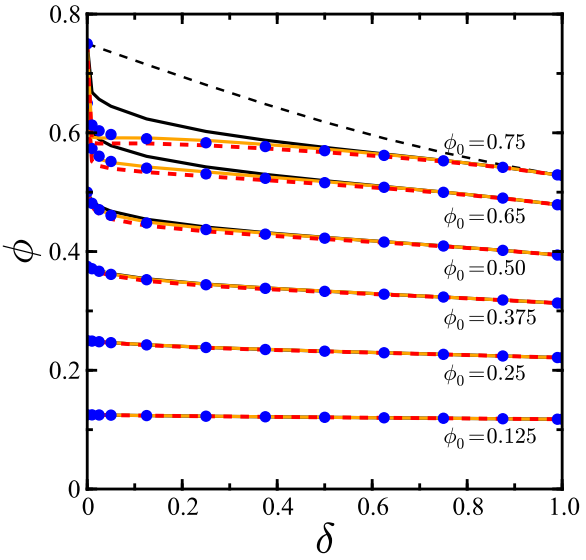

Fig. 8 The occupied volume fraction ϕ as a function of the penetration probability parameter δ in two dimension ($d = 2$). The ζ_V-SIM result is shown as a solid black curve. The result obtained using the *N*-SPA expression (dashed black) is shown only for $\phi_0 = 0.75$. All other labels and symbols correspond to those in Fig. 7.

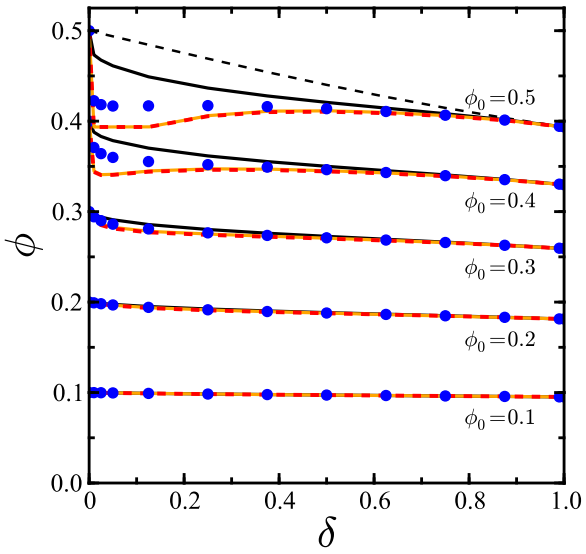

Fig. 9 The occupied volume fraction ϕ as a function of the penetration probability parameter δ in three dimensions ($d = 3$). The labeling and symbols correspond to those in Fig. 8. The result of the *N*-SPA expression (dashed black) is shown only for $\phi_0 = 0.5$.

negligible, typically $< 0.1\%$.

5.3 Three Dimensions

Figure 9 shows the results for ϕ measured from simulation and predicted by the analytic approaches of Sec. 4 for a system of three-dimensional spheres. At low to moderate densities $\phi_0 \in \{0.1, 0.2, 0.3\}$ the results from MD simulations agree with the ζ_V-SIM, ζ_L-SIM, and the ζ_L-SPA expressions across all ranges of δ. In this density regime, the error for all three expressions is $< 2\%$ at small δ values and is typically $< 1\%$ for $\delta \geq 0.25$.

At higher densities $\phi_0 \in \{0.4, 0.5\}$, close and above the HC freezing transition density ($\phi_0 \approx 0.491$), the theoretical predictions are in agreement with the MD results for large δ, contrary to the case of small δ. The latter divergence is caused by a change in structure from an isotropic state to a crystal or clustered state. Note that when $\zeta_L > 1$, which is shown in Fig. 4(c), the weighting of states in Eqs. (23) and (29) fails catastrophically. In this case, we make an *ad hoc* correction by imposing that ζ_L be bound from above by $\zeta_L = 1$. When clustering behavior dominates the structure of the system, it has been shown that for the deterministic PS potential (2) other analytic theories breakdown.[25,27] In this regime, completely overlapped states are highly favored and theory based on assumptions of spatial uniformity would be expected to fail. At high densities we observe in systems governed by the stochastic potential (6) the same *"cluster anomaly"* found in the deterministic (GEM-*n*) model.[56]

To characterize the anomalous clustered state, the dependence of the clustering probability on ϕ_0 was measured from MD simulations. Let $P_c(i)$ denote the probability of a randomly chosen particle being connected by overlaps to i other particles, self-inclusive.[27] If the particle does not overlap with any other particles ($i = 1$) it is a monomer; two penetrating particles form a dimer ($i = 2$) given there is no other particle overlapping the former ones, *etc*.

The results are shown in Fig. 10. At $\delta = 0$, no particles overlap and the system consists entirely of monomers. At small δ and large ϕ_0 the most probable configuration is a dimer. The turnover from a state in which monomers are favored to a state in which the particles cluster and dimers are favored is the exact trend of clustering observed in the (GEM-*n*) model (c.f. Fig. 4 in Ref. 56). For intermediate δ, higher order oligomers are formed and the distribution of clusters is Poisson-like as observed by comparing the middle and bottom panels of Fig. 10. For $\delta = 1$ the particles have no spatial correlation and are Poisson distributed.

The internal dimer radial distribution function $g_2^{\rm di}(r;\delta)$ gives the probability to find the second particle in a dimer at a distance r from the first particle. For $r > \sigma$, $g_2^{\rm di}(r;\delta) = 0$ as the two particles are not in a dimerized state in this case. In Fig. 11 the ratio $g_2^{\rm di}(r;\delta)/g_2^{\rm di}(\sigma^-;\delta)$ is shown for various δ values for $\phi_0 = 0.25$ and $\phi_0 = 0.5$. For $r \approx \sigma$, this ratio decreases because the cluster is more likely to be in a higher order oligomer due

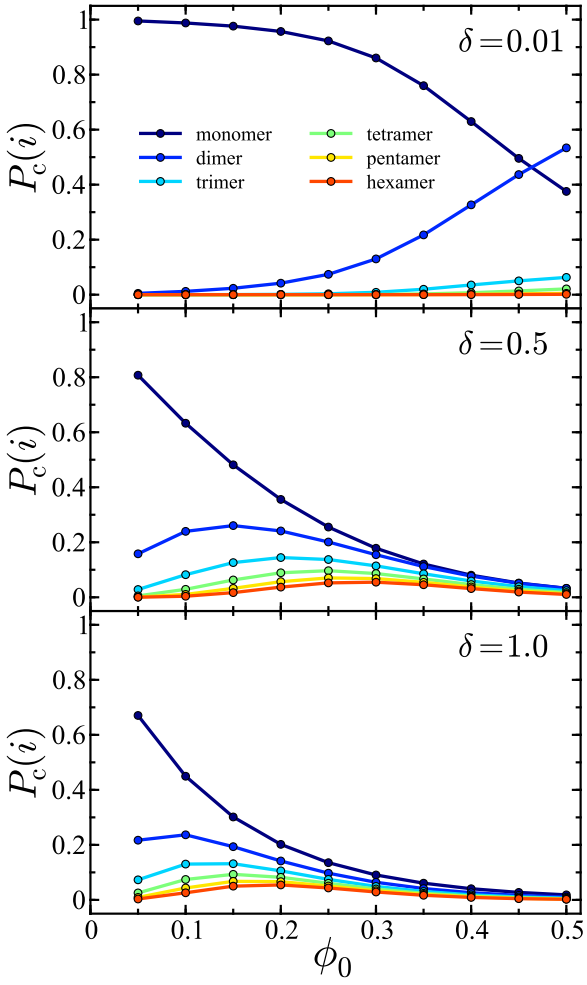

Fig. 10 The clustering probabilities $P_c(i)$ of three-dimensional spheres as a function of ϕ_0 for $\delta = 0.01$ (top), $\delta = 0.5$ (middle), and $\delta = 1$ (bottom). Different values of i run from "monomer" ($i = 1$) to "hexamer" ($i = 6$) as indicated in the top panel. For each set of parameters $\{\phi_0, \delta\}$ the probabilities were calculated by integrating over 5×10^5 spatial configurations.

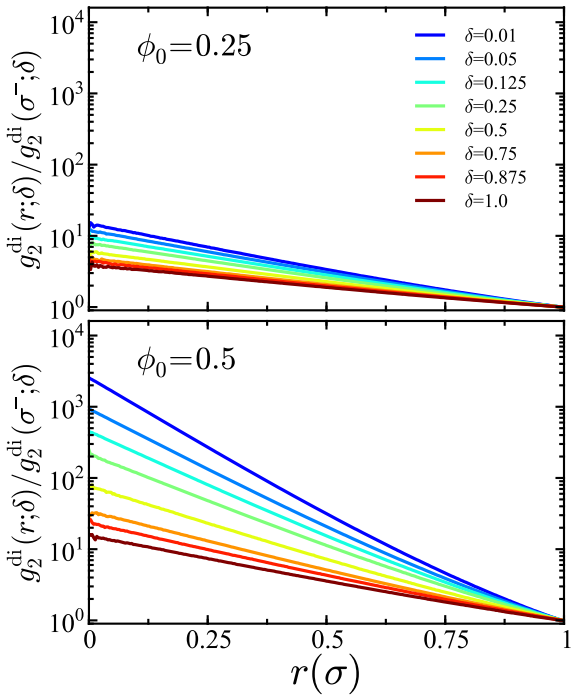

Fig. 11 Semi-log plots of the scaled internal dimer $g_2^{\rm di}(r;\delta)/g_2^{\rm di}(\sigma^-;\delta)$ radial distribution functions for three-dimensional spheres at $\phi_0 = 0.25$ (top) and $\phi_0 = 0.5$ (bottom).

to the available volume for other particles to occupy. As r approaches 0, the particles become completely overlapped. At $\phi_0 = 0.25$ and $\delta = 0.01$, the ratio $g_2^{\rm di}(0;\delta)/g_2^{\rm di}(\sigma^-;\delta) \approx 15$ while at $\phi_0 = 0.5$ and $\delta = 0.01$ it jumps up to ~ 2500 indicating a large increase in propensity for the dimer to be in a highly overlapped state.

6 Conclusions

We have studied the static structures of a system of stochastically penetrable spheres through MD simulations and analytic theory in dimensions one, two, and three. In simulation, the interactions between particles are governed by a stochastic potential. This stochastic potential bridges hard-core and ideal behavior through a penetration parameter δ. The value of δ governs whether the particles are allowed to interpenetrate (overlap) or are completely hard. When the particles take on overlapping states, the volume occupied by the system is reduced. To predict the particle volume fraction, analytic theories have been developed based on conditional probabilities derived from the sequential addition of particles to configuration space. The particle volume fraction has been measured from simulation and the results have been compared to the theoretical predictions. These results were found to be in excellent agreement apart from an observed clustered regime at

high densities and small δ in three dimensions. We have characterized this regime through analysis of clustering probabilities and intracluster spatial distributions.

In one and two dimensions, over the densities studied, we see no conclusive evidence of a transition from an isotropic stable state to a cluster-forming regime where particles exist, and persist, in completely overlapped states. Trends in the effective occupied volume fraction ϕ suggest that these transitions could be observed as the density is increased toward the maximum hard-core packing fraction.

A qualitative comparison between the simulation results generated from deterministic bounded models and the presented stochastic bounded model has shown that the stochastic models capture the general behavior of their deterministic analogs. In particular, the collective effect of pairwise soft interactions appear to be characterizable through a single reduced parameter that captures their overlap probability. We further conjecture that the structural properties of deterministic bounded potentials can be exactly reproduced using stochastic models based on this one characteristic. The derivation of stochastically realized, non-Newtonian equations of motion for coarse-grained macromolecular dynamics is a focus of our current research.

7 Acknowledgments

This work has been partially supported by the National Science Foundation (NSF) through Grant No. NSF-CHE-1112067.

References

1 J. F. Dama, A. V. Sinitskiy, M. McCullagh, J. Weare, B. Roux, A. R. Dinner and G. A. Voth, *J. Chem. Theory Comput.*, 2013, **9**, 2466–2480.
2 M. G. Saunders and G. A. Voth, *Annu. Rev. Biophys.*, 2013, **42**, 73–93.
3 W. G. Noid, *J. Chem. Phys.*, 2013, **139**, 090901.
4 C. N. Likos, *Soft Matter*, 2006, **2**, 478–498.
5 N. Koumakis, A. Pamvouxoglou, A. S. Poulos and G. Petekidis, *Soft Matter*, 2012, **8**, 4271–4284.
6 J. B. Miller, A. C. P. Usselman, R. J. Anthony, U. R. Kortshagen, A. J. Wagner, A. R. Denton and E. K. Hobbie, *Soft Matter*, 2014, **10**, 1665–1675.
7 H. Graf and H. Löwen, *Phys. Rev. E*, 1998, **57**, 5744–5753.
8 M. Schmidt and M. Fuchs, *J. Chem. Phys.*, 2002, **117**, 6308–6312.
9 J. C. Pamies, A. Cacciuto and D. Frenkel, *J. Chem. Phys.*, 2009, **131**, 044514.
10 C. N. Likos, S. Rosenfeldt, N. Dingenouts, M. Ballauff, P. Lindner, N. Werner and F. Vogtle, *J. Chem. Phys.*, 2002, **117**, 1869–1877.
11 B. Mladek, M. Fernaud, G. Kahl and M. Neumann, *Condens. Matter Phys.*, 2005, **8**, 135–148.
12 B. M. Mladek, D. Gottwald, G. Kahl, M. Neumann and C. N. Likos, *Phys. Rev. Lett.*, 2006, **96**, 045701.
13 F. Stillinger, *J. Chem. Phys.*, 1976, **65**, 3968–3974.
14 C. Zachary, F. Stillinger and S. Torquato, *J. Chem. Phys.*, 2008, **128**, 224505.
15 W. Krekelberg, T. Kumar, J. Mittal, J. Errington and T. Truskett, *Phys. Rev. E*, 2009, **79**, 031203.
16 A. Ikeda and K. Miyazaki, *Phys. Rev. Lett.*, 2011, **106**, 015701.
17 C. Marquest and T. Witten, *Journal de Physique*, 1989, **50**, 1267–1277.
18 D. Chandler, J. Weeks and H. Andersen, *Science*, 1983, **220**, 787–794.
19 A. V. Popov, J. Melvin and R. Hernandez, *J. Phys. Chem. A*, 2006, **110**, 1635–1644.
20 A. K. Tucker and R. Hernandez, *J. Phys. Chem. B*, 2012, **116**, 1328–1334.
21 A. Santos, *Phys. Rev. E*, 2012, **86**, 040102(R).
22 A. Santos and A. Malijevskỳ, *Phys. Rev. E*, 2007, **75**, 021201.
23 A. Malijevskỳ, S. Yuste and A. Santos, *Phys. Rev. E*, 2007, **76**, 021504.
24 A. Malijevsky and A. Santos, *J. Chem. Phys.*, 2006, **124**, 074508.
25 S. Suh, C. Kim, S. Kim and A. Santos, *Phys. Rev. E*, 2010, **82**, 051202.
26 N. Choudhury and S. Ghosh, *J. Chem. Phys.*, 2003, **119**, 4827–4832.
27 L. Viererblová, J. Kolafa, S. Labík and A. Malijevskỳ, *Phys. Chem. Chem. Phys.*, 2010, **12**, 254–262.
28 C. Likos, M. Watzlawek and H. Löwen, *Phys. Rev. E*, 1998, **58**, 3135–3144.
29 A. Santos, R. Fantoni and A. Giacometti, *Phys. Rev. E*, 2008, **77**, 051206.
30 R. Fantoni, A. Giacometti, A. Malijevskỳ and A. Santos, *J. Chem. Phys.*, 2009, **131**, 124106.
31 R. Fantoni, A. Malijevsk, A. Santos and A. Giacometti, *Mol. Phys.*, 2011, **109**, 2723–2736.
32 G. Malescio, *Mol. Phys.*, 2013, doi:10.1080/00268976.2013.860246.
33 Y. Chiew and E. Glandt, *J. Colloid Interface Sci.*, 1984, **99**, 86–96.
34 J. Quintanilla and S. Torquato, *Phys. Rev. E*, 1996, **54**, 4027–4036.
35 S. Torquato and G. Stell, *J. Chem. Phys.*, 1984, **80**, 878–880.
36 J. Quintanilla and S. Torquato, *Phys. Rev. E*, 1996, **54**, 5331–5339.
37 B. Widom, *J. Chem. Phys.*, 1971, **54**, 3950–3957.
38 S. Torquato and G. Stell, *J. Chem. Phys.*, 1983, **79**, 1505–1510.
39 K. Gotoh, M. Nakagawa, M. Furuuchi and A. Yoshigi, *J. Chem. Phys.*, 1986, **85**, 3078–3080.
40 S. Torquato, *Random Heterogenous Materials: Microstructure and Macroscopic Properties*, Springer-Verlag, New York, 2002.
41 S. Suh, W. Min and J. MacElroy, *Bull. Korean Chem. Soc.*, 1999, **20**, 1521–1523.
42 S. Lee and S. Torquato, *J. Chem. Phys.*, 1988, **89**, 3258–3263.
43 M.-J. Fernaud, E. Lomba and L. L. Lee, *J. Chem. Phys.*, 2000, **112**, 810–816.
44 S. Kim and S. Suh, *J. Chem. Phys.*, 2002, **117**, 9880–9886.
45 L. Blum and G. Stell, *J. Chem. Phys.*, 1979, **71**, 42–46.
46 G. T. Craven, A. V. Popov and R. Hernandez, *J. Chem. Phys.*, 2013, **138**, 244901.
47 M. P. Allen and D. J. Tildesley, *Computer Simulations of Liquids*, Oxford, New York, 1987.
48 L. Van Hove, *Physica*, 1950, **16**, 137–143.
49 A. Jaster, *Phys. Lett. A*, 2004, **330**, 120 – 125.
50 C. H. Mak, *Phys. Rev. E*, 2006, **73**, 065104.
51 W. G. Hoover and F. H. Ree, *J. Chem. Phys.*, 1968, **49**, 3609–3617.
52 C. Vega and E. G. Noya, *J. Chem. Phys.*, 2007, **127**, 154113.
53 E. G. Noya, C. Vega and E. de Miguel, *J. Chem. Phys.*, 2008, **128**, 154507.
54 B. M. Mladek, P. Charbonneau, C. N. Likos, D. Frenkel and G. Kahl, *J. Phys.: Condens. Matter*, 2008, **20**, 494245.
55 K. Zhang and P. Charbonneau, *J. Chem. Phys.*, 2012, **136**, 214106.
56 D. Coslovich and A. Ikeda, *Soft Matter*, 2013, **9**, 6786–6795.
57 A. Elsner, A. Wagner, T. Aste, H. Hermann and D. Stoyan, *J. Phys. Chem. B*, 2009, **113**, 7780–7784.
58 U. Brodatzki and K. Mecke, *Comp. Phys. Comm.*, 2002, **147**, 218–221.
59 P. Rikvold and G. Stell, *J. Colloid Interface Sci.*, 1985, **108**, 158–173.
60 P. Rikvold and G. Stell, *J. Chem. Phys.*, 1985, **82**, 1014–1020.

61 J. Kirkwood, *J. Chem. Phys.*, 1935, **3**, 300–313.
62 S. Torquato, B. Lu and J. Rubinstein, *Phys. Rev. A*, 1990, **41**, 2059–2075.